STRUCTURAL, MORPHOLOGICAL, AND PHOTOLUMINESCENCE PROPERTIES OF TiO_2-DOPED CdO NANOCOMPOSITES PREPARED BY A SIMPLE SOLUTION METHOD**

M. Seshu Kumar [1], R. V. S. S. N. Ravikumar [2], M. C. Rao [1*]

[1] Department of Physics, Andhra Loyola College, Vijayawada, India; e-mail: raomc72@gmail.com
[2] Department of Physics, Acharya Nagarjuna University, Nagarjuna Nagar, Guntur, India

Pure CdO and TiO_2-doped CdO nanocomposites with different wt% ratios (0.1, 0.3, and 0.5%) were prepared by a simple solution method. Structural, morphological, and elemental composition of the prepared samples was undertaken by X-ray diffraction, scanning electron microscopy (SEM), energy dispersive X-ray analysis, and photoluminescence. The diffraction peaks of the samples showed the cubic phase structure and the prepared nanocomposites were on the nanoscale. SEM revealed the plate-like chunks with irregular grains due to agglomeration. The particle size of the pure CdO sample was found to be 61.98 nm, whereas TiO_2-doped CdO (0.1, 0.3, and 0.5%) exhibited 49.57, 35.41, and 31 nm. The first peak was observed at 1.90 eV in the IR-visible region and the second peak at 2.38 eV. Both the peaks correspond to CdO. Near-band-edge emission of 2.38 eV is typical for both pure and doped CdO. It can be suggested that the photo-generated electrons have been trapped in to Ti^{4+} in the forbidden gap, which enhanced the deep level emission.

Keywords: *TiO_2-doped CdO, X-ray diffraction, scanning electron microscopy, energy dispersive X-ray, photoluminescence.*

СТРУКТУРНЫЕ, МОРФОЛОГИЧЕСКИЕ И ФОТОЛЮМИНЕСЦЕНТНЫЕ СВОЙСТВА ПОЛУЧЕННЫХ МЕТОДОМ ПРОСТОГО РАСТВОРЕНИЯ НАНОКОМПОЗИТОВ CdO, ЛЕГИРОВАННЫХ TiO_2

M. S. Kumar [1], R. V. S. S. N. Ravikumar [2], M. C. Rao [1*]

УДК 539.261;535.37;620.3

[1] Колледж Андхра Лойола, Виджаявада, Индия; e-mail: raomc72@gmail.com
[2] Университет Ачарьи Нагарджуны, Нагарджуна Нагар, Гунтур, Индия

(Поступила 19 апреля 2022)

Чистый CdO и нанокомпозиты CdO, легированные TiO_2 (0.1, 0.3 и 0.5 мас.%), приготовлены методом простого растворения. Структурный, морфологический и элементный составы определены методами рентгеновской дифракции, сканирующей электронной микроскопии (SEM), энергодисперсионного рентгеноструктурного анализа и фотолюминесценции. На дифрактограммах видно, что образцы имеют кубическую фазовую структуру, а нанокомпозиты — наномасштаб. С помощью SEM выявлены пластинчатые участки с неравномерной зернистостью вследствие агломерации. Размеры частиц чистого CdO 61.98 нм, а CdO, легированного TiO_2 (0.1, 0.3 и 0.5 мас.%), — 49.57, 35.41 и 31 нм. Максимумы при 1.90 и 2.38 эВ в ИК-видимой области соответствуют CdO. Близкраевое излучение при 2.38 эВ характерно как для чистого, так и для легированного CdO. Можно предположить, что фотогенерированные электроны захватываются Ti^{4+} в запрещенной зоне, что усиливает излучение глубоких уровней.

Ключевые слова: *CdO, легированный TiO_2; рентгеновская дифракция; сканирующая электронная микроскопия; энергодисперсионный рентгеноструктурный анализ; фотолюминесценция.*

**Full text is published in JAS V. 90, No. 1 (http://springer.com/journal/10812) and in electronic version of ZhPS V. 90, No. 1 (http://www.elibrary.ru/title_about.asp?id=7318; sales@elibrary.ru).

Introduction. Scientific researchers have paid much attention to water contamination, and the necessity of world energy these days in relation to energy storage devices with high performance. In recent years, super capacitors were found to have many advantages compared with energy storage devices owing to excellent features such as high energy density, large power density, faster recharge capacity, and longer life [1]. The performance of the super capacitors depends on the properties of electrode materials. Semiconductor metal oxides such as CdO, TiO_2, and ZnO are used in optoelectronic device applications such as photocatalyst and sensing elements [2–4]. The electrode materials of transition metal oxides improve the supercapacitor energy and power density [5]. The bandgap of CdO varies from 2.2 to 2.3 eV [6]. CdO (2.2 eV) has been reported to be an important semiconductor for the wastewater treatment of organic pollutants [7]. Because of these special characteristics, it is used in gas sensors, solar cells, laser, spintronics, etc. [8–18]. Owing to its unique physical and chemical properties, it is used in commercial device applications as IR detectors, anti-reflection coatings, phototransistors, and liquid crystal displays. Owing to the presence of interstitial cadmium and oxygen ions and high intrinsic durability, CdO materials possess high electrical conductivity. Cadmium oxide nanocomposites are used as super electrodes owing to their toxic nature.

Among the various transition metal oxides, titanium oxide is a stunning electrode material. It is used in commercial applications owing to high specific capacitance and magnificent cycle-life stability [19]. The TiO_2 material is highly transparent in the visible region [20]. In the present work, the simple solution method is used for the synthesis of CdO nanocomposites. The main aspect of the present study is to prepare the nanocomposites in a simple and cost-effective method. The outcome of the results shows potential application in the preparation of energy storage devices.

Experimental. Cadmium nitrate ($Cd(NO_3)_2$), titanium dioxide (TiO_2), cadmium hydroxide (CdOH), and methanol (CH_3OH) from Sigma Aldrich, India, were used. The CdO solution was prepared by dissolving an appropriate amount of $Cd(NO_3)_2$ in the presence of CdOH and CH_3OH at room temperature. A solution (20 mL) containing 0.1M $Cd(NO_3)_2$ in CH_3OH was added dropwise to 100 mL of 0.1 M CdOH and then stirred for 30 min. Distilled water was added to the obtained solution in the ratio 0.04 and the solution was stirred continuously for up to 30 min. Further, the obtained solution was kept under refrigeration for 2 h, for centrifugation. After the formation of precipitate, it was washed with distilled water several times and then dried at room temperature for more than 24 h, and finally it was calcinated at 450 and 650^{o}C for 2 h by heating at a rate of 15^o per min.

From the Bruker X-ray diffractometer, X-ray diffraction (XRD) patterns of the sample were recorded by using CuK_α as radiation with a scan rate of 20° per min. Surface morphology and energy dispersive X-ray analysis (EDX) of the prepared nanocomposites were characterized by a Neon 40 Crossbeam (Carl Zeiss, Germany). For the synthesized sample, photoluminescence (PL) studies were recorded with a 450-W Light Xenon Source on JobinYvonFluorimeter-FL3-11 Spectrofluorometer.

Results and discussion. For the synthesized samples of pure CdO and TiO_2-doped CdO nanocomposites, XRD patterns were recorded and shown in Fig.1. The XRD patterns corresponding to 2θ values appeared at 33.1, 38.4, 55.4, 66.1, 69.2, and 82.1° indicating (1 0 0), (0 0 2), (1 0 1), (2 2 0), (3 1 1), and (2 2 2) reflections, respectively. The pure and TiO_2-doped CdO has a face-centered cubic structure, because of stronger intensity peaks at 33.1 and 38.4°, corresponding to the values of 2θ. Owing to TiO_2 doping, the intensities of the peaks are changed. From the recorded data, it was confirmed that the phase in CdO is single, which coincides with JCDPS card No.78-0592. Using Scherrer's equation, the full width at half maximum (FWHM) and the crystalline size of the samples can be calculated with the help of the XRD pattern [21]:

$$D = 0.9\lambda/(\beta\cos\theta). \quad (1)$$

The XRD peak value of FWHM is represented by β, and θ is the diffracting angle.

The morphological features of pure CdO sample represent irregular grains. They were shown in Fig. 2a by an SEM image. The samples of nanocomposites at higher concentrations of TiO_2 doping were observed through the micrographs of Fig. 2b–d. The presence of CdO containing sample forms plate-like chunks. The nanoparticles, which are accumulated on the surface, form intensified plates [22]. From the EDX analysis, the elemental and chemical compositions are estimated and presented in Fig. 2a–d. As the agglomeration increases, the number of nanoparticles also increases. The sample content of CdO characteristic peaks represents the confirmation of Cd, Ti, and O. From the EDS data, the nanocomposite samples represent the percentage increment in the TiO_2-doped CdO. The XRD results are consistent with EDX data.

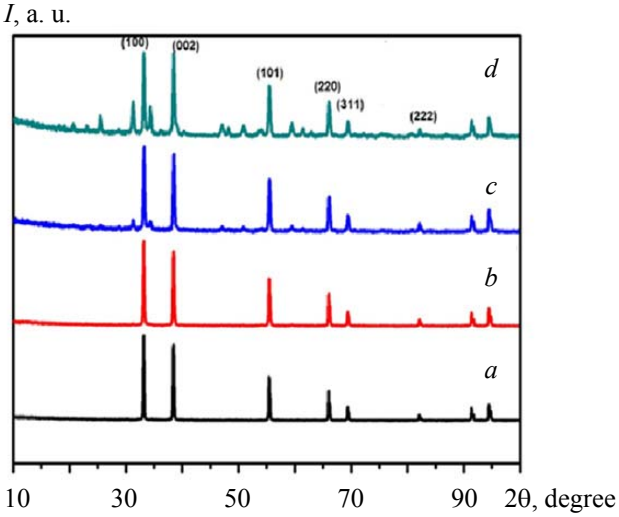

Fig. 1. XRD pattern of (a) pure CdO, TiO_2-doped CdO for (b) 0.1%, (c) 0.3%, and (d) 0.5%.

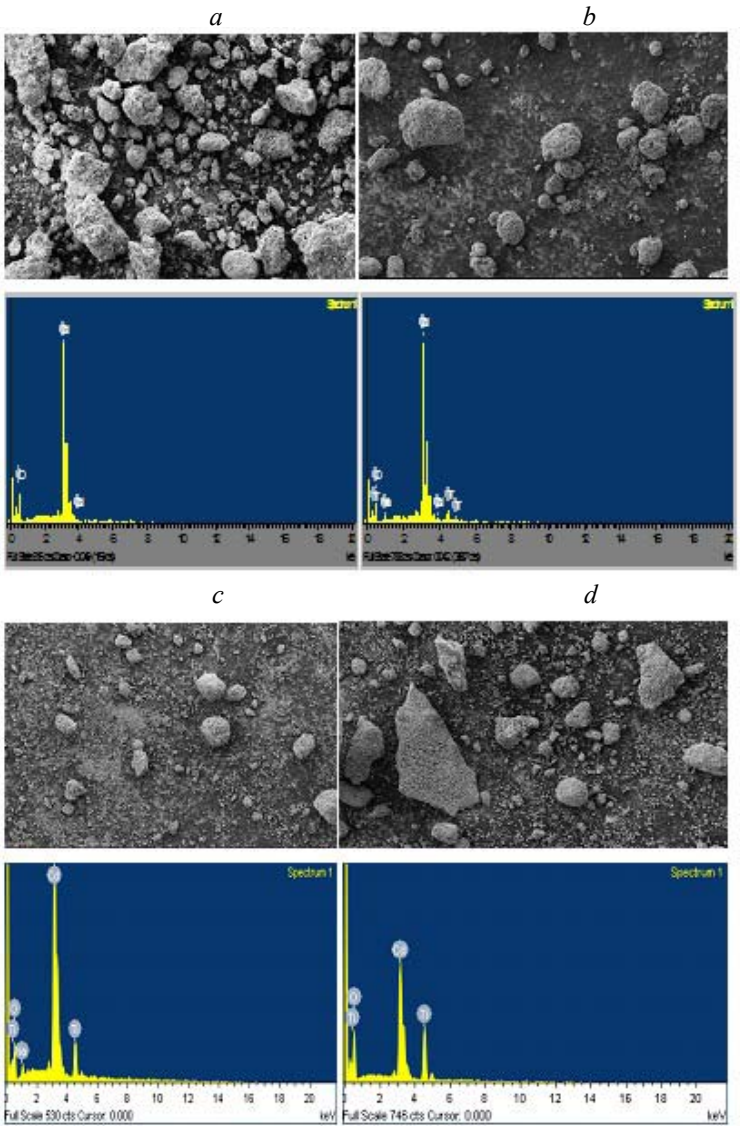

Fig. 2. SEM and EDX images of (a) pure CdO, TiO_2-doped CdO for (b) 0.1%, (c) 0.3%, and (d) 0.5%.

The microstrain behavior of the CdO phase observed in the samples gives the relation between βcosθ and 4sinθ. It forms a straight line and is equal to its slope. It is shown in Fig. 3. The *y*-intercept of the prepared sample is found to be 0.00175, 0.0021, 0.0028, and 0.0032 and the particle size of the pure CdO is found to be 61.98 nm, whereas TiO_2-doped CdO (0.1, 0.3, and 0.5%) are at 49.57, 35.41, and 31 nm. The particle size of the samples clearly shows the decrement in the size on increasing TiO_2 percentage [23, 24]. It is found that the grain size of the TiO_2-doped CdO samples decreases with an expansion in the Ti content. This is presumably due to the Ti ions lessening the crystallinity of the CdO. The relation between the crystallite size and dislocation density is represented by [23, 25, 26]:

$$\delta = 1/D^2, \quad (2)$$

where D is the crystallite size and δ is the dislocation density. The obtained values of the crystallite size of the samples are in good agreement with XRD data.

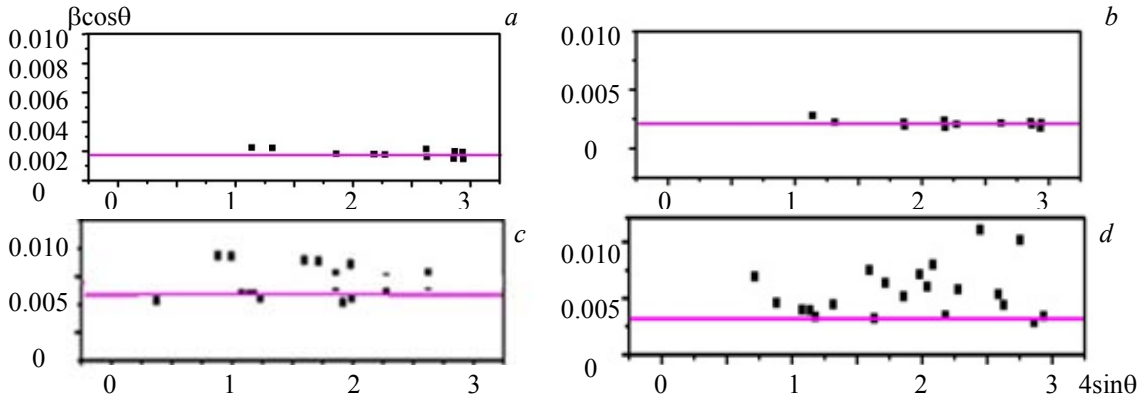

Fig. 3. W-H analysis of (a) pure CdO, TiO_2-doped CdO for (b) 0.1%, (c) 0.3%, and (d) 0.5%.

Photoluminescence study is an authoritative characterization method of determining the electronic structure, recombination of the electron-hole pair, and the energy band level of the nanocomposites. Photoluminescence spectra give information about the intensity of emitted radiation as a function of either the excitation wavelength or the emission wavelength. The intensity of the light is plotted against the energy on the spectrum. Figure 4 shows the recordings of pure and TiO_2-doped CdO at room temperature. From the PL spectra, two peaks are observed. The first peak is observed at 1.90 eV in the IR-visible region and the second peak is at 2.38 eV. Both the peaks correspond to CdO. Near-band-edge emission of 2.38 eV is typical for both pure and doped CdO. The fact that its intensity (as well as the intensity of radiation from deep levels) increases with the doping level may testify to a decrease in the concentration of nonradiative centers as a result of doping [27]. The interpretation of the emission band of deep centers (1.9 eV) raises no particular objections, although with a growth of the doping level, an increase in the intensity of both bands is observed. This indicates a decrease in the concentration of nonradiative centers rather than an increase in the

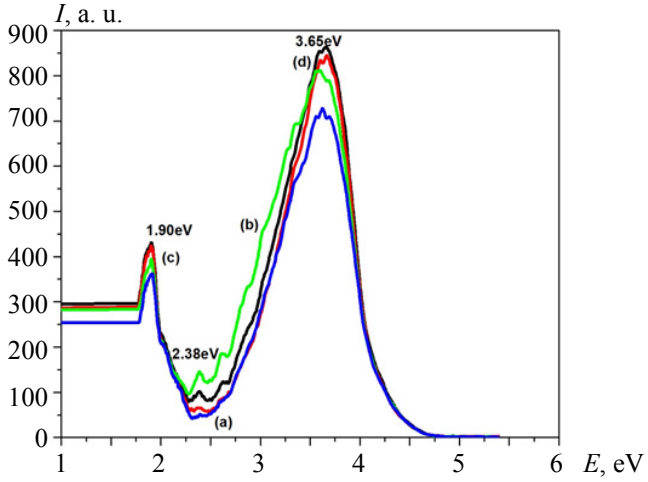

Fig. 4. PL spectra of (a) pure CdO, TiO_2-doped CdO for (b) 0.1%, (c) 0.3%, and (d) 0.5%.

concentration of deep centers [28]. The peak at 3.65 eV is due to the contaminations present in the synthesized sample. It can be suggested that the photo-generated electrons might have been trapped in Ti^{4+} in the forbidden gap, which enhanced the deep level emission. Ti^{4+} that occupied the Cd^{2+} site in the lattice structure can trap the electrons that come back from the conduction band to the valence band. This refers to the large positive charge of Ti^{4+} [29].

Conclusions. TiO_2-doped CdO nanocomposites were prepared by a simple solution technique. From the X-ray diffraction patterns, the prepared nanocomposite was within the nanoscale range. The presence of CdO forms plate-like chunks. The nanoparticles accumulated on the surface form-intensified plates. The particle size of the pure CdO was found to be 61.98 nm, whereas TiO_2-doped CdO (0.1, 0.3, and 0.5%) were at 49.57, 35.41, and 31 nm. The photoluminescence spectra showed two peaks. The first peak is observed at 1.90 eV in the IR-visible region and the second peak is at 2.38 eV. Both the peaks correspond to CdO. Near-band-edge emission of 2.38 eV is typical of both pure and doped CdO. It can be suggested that the photo-generated electrons might have been trapped in Ti^{4+} in the forbidden gap, which enhanced the deep level emission. Ti^{4+} that occupied the Cd^{2+} site in the lattice structure can trap the electrons that come back from the conduction band to the valence band. The expected outcomes of the present work are suitable for the development of display devices and optoelectronic gadget applications.

REFERENCES

1. C. Aydın, H. M. El-Nasser, F. Yakuphanoglu, I. S. Yahia, M. Aksoy, *J. Alloys Compd*., **509**, 854–858 (2011).
2. M. H. Vijaykumar, P. A. Vaishampayan, Y. S. Shouche, T. B. Karegoudar, *Enzym. Microbiol. Tech*., **40**, No. 2, 204–211 (2007).
3. S. Balachandran, S. G. Praveen, R. Velmurugan, M. Swaminathan, *RSC Adv*., **4**, 4353–4362 (2014).
4. T. O. Mahony, E. Guibal, J. M. Tobin, *Enzym. Microbiol. Tech*., **31**, 456–463 (2002).
5. S. Aksoy, Y. Caglar, S. Ilican, M. Caglar, *Int. J. Hydrogen Energy*, **3**, No. 4, 5191–5195 (2009).
6. S. K. Vasheghani Farahani, V. Muñoz-Sanjosé, J. Zúñiga-Pérez, C. F. McConville, T. D. Veal, *Appl. Phys. Lett*., **102**, 022102 (2013).
7. S. Kumar, M. Selvakumar Babu, G. Karuthapandian, S. Chattopadhyay, *Mater. Lett*., **151**, 45–48 (2015).
8. D. Zhang, Y. Zhang, H. Ma, H. Yan, Y. Song, *Mater. Chem. Phys*., **144**, No. 3, 369–376 (2009).
9. Y. Su, A. S. Adeleye, Y. Huang, X. Sun, C. Dai, *Water Res*., **63**, 102–111 (2014).
10. K. Mukesh Sharma, J. Narayanan, K. Sanjay Upadhyay, A. Goel, *Biosen. Bioelect*., **74**, 299–304 (2015).
11. F. Yakuphanoglu, *Solar Energy*, **85**, No. 11, 2704–2709 (2011).
12. S. T. Hossain, S. K. Mukherjee, *J. Hazard Mater*., **260**, 1073–1082 (2013).
13. I. R. Chávez Urbiola, R. Ramírez Bon, Y. V. Vorobiev, *Thin Solid Films*, **592**, 110–117 (2015).
14. S. Sivakumar, A. Venkatesan, P. Soundhirarajan, C. P. Khatiwada, *Spectrochim. Acta A: Mol. Biomol. Spectrosc*., **136**, 1751–1759 (2015).
15. J. L. Jiménez-Pérez, F. R. Gutiérrez, R. Sánchez-Sosa, M. G. Zapata, Z. N. Torres, C. Pacheco, *Mater. Sci. Semicond. Proc*., **37**, 62–67 (2015).
16. C. C. Vidyasagar, Y. Arthoba Naik, T. G. Venkatesh, R. Viswanatha, *Powder Tech*., **214**, No. 3, 337–343 (2011).
17. S. R. Chowdhury, E. K. Yanful, *J. Environ. Management*, **129**, 642–651 (2013).
18. K. R. Murali, A. Kalaivanan, S. Perumal, N. Neelakand Pillai, *J. Alloys Compd*., **503**, 350–353 (2010).
19. R. C. Weast, S. M. Selby, Hand Book "Chemistry and Physics in CRC", 3rd ed. (1966–1976).
20. E. K. Abdul-Hussein, A. M. Hayder, A. I. Khudiar, *J. Mater. Res. Tech*., **2**, No. 2, 182–187 (2013).
21. A. Wang, J. R. Babcock, N. L. Edleman, A. W. Metz, M. A. Lane, R. Asahi, V. P. Dravid, C. R. Kannewurf, *Proc. Nat. Acad. Sci. USA*, **98**, 7113–7116 (2001).
22. O. Lupan, T. Pauporté, T. Le Bahers, I. Ciofini, B. Viana, *J. Phys. Chem. C*, **115**, 14548–14558 (2011).
23. F. Essam, Z. Abo, A. Ibrahem, B. Ibrahem, A. Atif Mossad, A. A. Walied Mohamed, *Res. Phys*., **12**, 562–570 (2019).
24. M. Iniya Pratheepa, M. Lawrence, *Vacuum*, **162**, 208–213 (2019).
25. P. Rajeswari, S. Dhanuskodi, *Cryst. Res. Technol*., **48**, No. 1, 589–598 (2013).
26. V. Radhika, V. Annamalai, G. Vijaya, D. Annakkodi, *J. Environ. Nanotechnol*., **5**, No. 3, 39–43 (2016).
27. K. T.-Jun, M. H. Huang, *J. Phys. Chem. B*, **110**, 13717–13721 (2006).
28. M. Ghosh, C. N. R. Rao, *Chem. Phys. Lett*., **393**, No. 4, 493–497 (2004).
29. S. A. Bidier, M. R. Hashim, M. Bououdina, *J. Mater. Sci. Mater. Electron*., **28**, 11178–11185 (2017).